Magazine of Civil Engineering

ISSN 2712-8172

journal homepage: http://engstroy.spbstu.ru/

DOI: 10.34910/MCE.106.6

Porosity of autoclave aerated concrete and foam concrete: origin of porosity and pore size

***K.A. Kurochkina**[*a], **L.A. Suleimanova**[a], **A.S. Kolomatsky**[b]

[a] *V.G. Shukhov Belgorod State Technological University, Belgorod, Russia*

[b] *Belgorod National Research University, Belgorod, Russia*

**E-mail: karina200386@yandex.ru*

Keywords: porosity, bubble, pore size, autoclaved aerated concrete, foam concrete

Abstract. Porosity in the hardening system consists of air cells, which are the main element of the cellular concrete structure and that formed when gas emission in the mixture or during the foaming. The paper presents the developed models of porous structure formation in autoclaved aerated concrete (AAC) and foam concrete (FC). We elaborated the concept of bubble porosity in fresh concrete by distinguishing three types of bubble pores: microbubble pores, membrane pores and cellular pores. The sizes of such pores are determined and the possibility of pore shape deformation is evaluated. The study revealed that capillary and hydrostatic pressure are the essential factors in the process of bubble system formation. Reducing the size of deformable cellular bubbles and obtaining an increased number of non-deformable membrane bubbles improves the AAC and FC structure. This is a promising method of improving AAC and FC production technology.

1. Introduction

The pore size and the porosity nature are essential for the most hydration hardening materials. By creating a porous structure in production process, highly effective inorganic materials for construction purposes are made from autoclaved aerated concrete (AAC) and foam concrete (FC) non-autoclaved of hardening [1–4].

Three types of pores in hardening systems are distinguished: gel pores, capillary pores and air pores. Air pores called cellular pores, gas pores, or macropores. The concepts of gel porosity were developed in [5]. Gel pores are a space in aggregated growth between highly dispersed hydrated phases. Capillary pores are the space occupied by the mixing water remaining after hydration, minus gel porosity. Gel porosity and capillary porosity mainly depends on the type and amount of binders in the initial mix, as well as the water to binder ratio [6–10]. Such pores will appear in the interbubble septa after matrix crystallization structure formation.

The cellular porosity in the hardening system is created by gas evolution in the mix or by foaming [11–15]. In AAC technology a highly mobile mixture is converted into a raw mass with a coagulation structure due to two quick chemical reactions. In the reaction with dispersed aluminum, hydrogen is emitted and $3CaO{\cdot}Al_2O_3{\cdot}6H_2O$ is formed, and CaO hydrates into $Ca(OH)_2$, binding part of the mixing water into the solid phase. FC technologies are based on three-phase foam production with air bubbles as a dispersed phase of the system [1].

Raw density, strength, thermal conductivity and other properties of AAC [16, 17] and FC [18, 19] are interrelated. Data on the porous structure of the material are used when cellular concrete of the same

Kurochkina, K.A., Suleimanova, L.A., Kolomatsky, A.S. Porosity of autoclave aerated concrete and foam concrete: origin of porosity and pore size. Magazine of Civil Engineering. 2021. 106(6). Article No. 10606. DOI: 10.34910/MCE.106.6

density have different properties [20], when modeling porosity [21–24], when the nature of the processes in the hardening system is revealed [17, 25] and in other studies. The quantity and quality of bubble pores affects the properties of not only AAC and FC, but also other aerated concretes, for example, gypsum compositions [26–28]. Thermophysical characteristics of AAC and other cellular materials are important for building envelopes in connection with the relevance of energy saving issues for space heating [29–32].

Common to AAC and FC is the formation of their porous structure in a three-phase bubble system. Three-phase foam is both a FC mix and foam stabilized by fine particulate matter, for example [33–36]. The three-phase system of AAC and FC freshly prepared mixes can be reduced to a two-phase system, considering the bubble as a discrete phase, and a concentrated suspension as a carrier, condensed phase. The gas-liquid systems mechanics describes the processes in many modern technologies and is used to consider bubble porosity nature in a cellular concrete mixes [37]. The identification of the types, shapes and sizes of bubble pores in cellular concrete has a significant role for AAC and FC technology. The concept of bubble pores is significant for obtaining scientific data [38–40] and computer modeling of porous systems [41, 42].

According to the above mentioned aspects, the purpose of this study is to develop ideas about the origin of bubble porosity in aerated concrete and pore sizes in AAC and FC. The research tasks included modeling the porosity in AAC and FC, analyzing the bubble porosity taking into account the size of the bubble, and identifying factors that determine the formation of the bubble system. Consideration of the hardening system as a composition consisting of a matrix and bubbles allows one model to characterize the porous structure of different materials hardening AAC and FC. The division of bubble pores into species not only develops the existing understanding of the porosity of hardening systems, but also provides guidance for improving the cellular concrete technology.

2. Materials and Experimental method

2.1. Materials

It was studied FC pressure of the density class of D250 manufactured by LLC «Ecostroymaterials» from samples taken during the installation of monolithic thermal insulation of attic floors of buildings and AAC density class of D500 of CJSC «AEROBEL». The sampling was carried out simultaneously with the routine testing of the material properties by the enterprise. AAC had a dry density of 493 kg/m^3, pressure strands 5.54 N/mm^2, and a coefficient of thermal conductivity of 0.112 W/(mK). FC characteristics: dry density 238 kg/m^3, compressive strength 0.64 MPa, coefficient of thermal conductivity 0.057 W/(mK).

2.2. Experimental method

The porous structure was evaluated visually on samples and on photographs on chips and sections. It was used a TESCAN MIRA 3 LMU scanning electron microscope (SEM) scan with an increase from 2 to 1.000.000 and an energy dispersive microanalysis with an attachment to the microscope of the spectrometer.

2.3. Modeling

Processes modeling occurring in porous hardening systems with a change in solid phases composition and ingredients aggregation state was carried out on silicate AAC mix with a density class of 500 kg/m^3 (D500). The manufacturing process of AAC according to the criterion of phase transformations is divided into three stages and two phase transformations in the system, which determine the staging (Fig. 1).

The characteristics of the model AAC mix according are given in the table. The lime and aluminum powder activity is taken equal to 100%. For the production of 1 m^3 of white AAC, 432.19 l of a AAC mixe with a water solid (W/S) ratio W/S = 0.6 is required. The volume fraction of the solid phase in the freshly prepared AAC mix is 0.375, the liquid phase is 0.625. Water in the AAC mix as a dispersion medium ensures the continuity of the hardening system.

Table. Silicate AAC mix characteristic with D500.

Characteristic	Mix ingredients			
	Lime	Quartz sand	Aluminum powder	Water
Proportions (kg on 1 m^3)	112	340	0.5	270
Density (kg/m^3)	3320	2650	2700	1000
Volumetric content of ingredients (l/m^3)	33.7	128.3	0.19	270

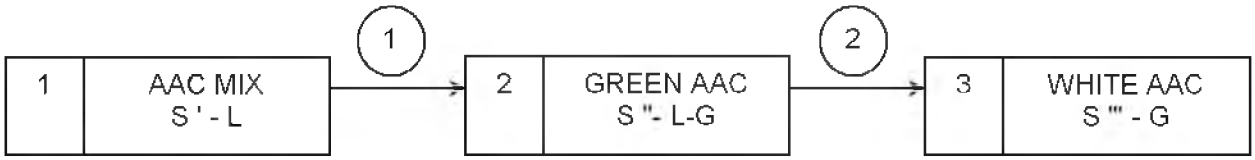

Figure 1. Manufacturing AAC process formalization:
□ – stages; ◯ – phase transformations;
S', S", S"' – solid phases composition, L – liquid phase, G – gas phase.

Bubble porosity of the adobe AAC cake is formed by the released gaseous hydrogen. Based on 1 m^3 of AAC we have:

$$V_B + \sum \frac{m_i}{\rho_i} + W^* = 1, \quad (1)$$

where V_B is bubble porosity volume, m^3/m^3; m_i is solid phases masses, kg; ρ_i is solid phases density, kg/m^3; W^* is mixing water volume minus solid phase bound, m^3/m^3.

The water in the green AAC cake in the second stage of system hardening remains a dispersion medium. Together with silica (SiO_2) and hydrated growth ($Ca(OH)_2$ and $3CaO \cdot Al_2O_3 \cdot 6H_2O$), water provides stability to membranes and the bubble system as a whole. The contraction porosity estimation during the portlandite formation for the considered model of AAC mix gives the value $5.36 \cdot 10^{-3}$ m^3/m^3.

In the process of green cake autoclave hardening at the second stage of phase transformations (Fig. 1), the physical and mechanical properties of AAC are formed. It is accepted that tobermorite $5CaO \cdot 6SiO_2 \cdot 5H_2O$ with density 2440 kg/m^3 is formed in the model system during hardening. Water at the end of autoclaving exhausts its functions. The volume fraction of the space occupied in green cake water becomes a source of capillary and gel porosity in AAC.

The gas bubbles growth in the freshly prepared mix during the green cake structure formation describes the Rayleigh-Plesset equation [34]:

$$P_G + P_{WV} \geq P_A + \rho_{mix} g H + \rho_{mix} \left(R\ddot{R} + \frac{3}{2}\dot{R}^2 \right) + \frac{2\sigma}{R} + \frac{4\eta\dot{R}}{R} + P_E, \quad (2)$$

where P_G и P_{WV} is gas and water vapor pressure in a bubble; P_A и P_E is atmospheric and excess pressures over the mix; ρ_{mix} is mix density; H is mix column height above the bubble; R is bubble radius; $\dot{R}$ and $\ddot{R}$ is speed and acceleration during bubble growth; σ is surface tension; η is viscosity.

Under conditions of metastable equilibrium for the formed bubble system in the expanded mix from equations (1) and (2) at atmospheric pressure, and also based on the relationship of pressure, volume and temperature of the gas phase, we obtain:

$$\frac{c \cdot K \cdot T_B}{P_A + \rho_{mix} \cdot g \cdot H + 2\sigma / R} + \sum \frac{m_i}{\rho_i} + W^* = 1, \quad (3)$$

where T_B is gas phase temperature in a bubble; c is proportionality coefficient; K is gas constant.

Significant indicators for bubble porosity in the green AAC cake structure formation are gas phase temperature, capillary and hydrostatic pressure.

3. Results and Discussion

Change in phase composition and porosity in a three-stage process according to Fig. 1 for a model AAC mix are presented in Fig. 2. In Fig. 3 a fragment of AAC structure D500 is shown, which according to the main elements corresponds to a model aerated concrete. In hardening systems, when water is bound to the solid phase, chemical shrinkage is observed. The value of the microporosity of the matrix due to chemical shrinkage can only be estimated by calculation according to the reaction equations. When removing water from a hardened cement paste, drying shrinkage takes place. The chemical shrinkage and drying shrinkage (Fig. 2) together give a total shrink of less than 1 % [43, 44]. When considering volumetric phase ratios and porosity in AAC and FC, the phenomena of shrinkage due to their small size can be ignored. Based on the concepts of hardening system porosity, size regions of gel and capillary pores are distinguished, and types, shape and sizes are substantiated for air (bubble) pores.

Five pore areas for AAC and FC were determined by the pore size criterion.

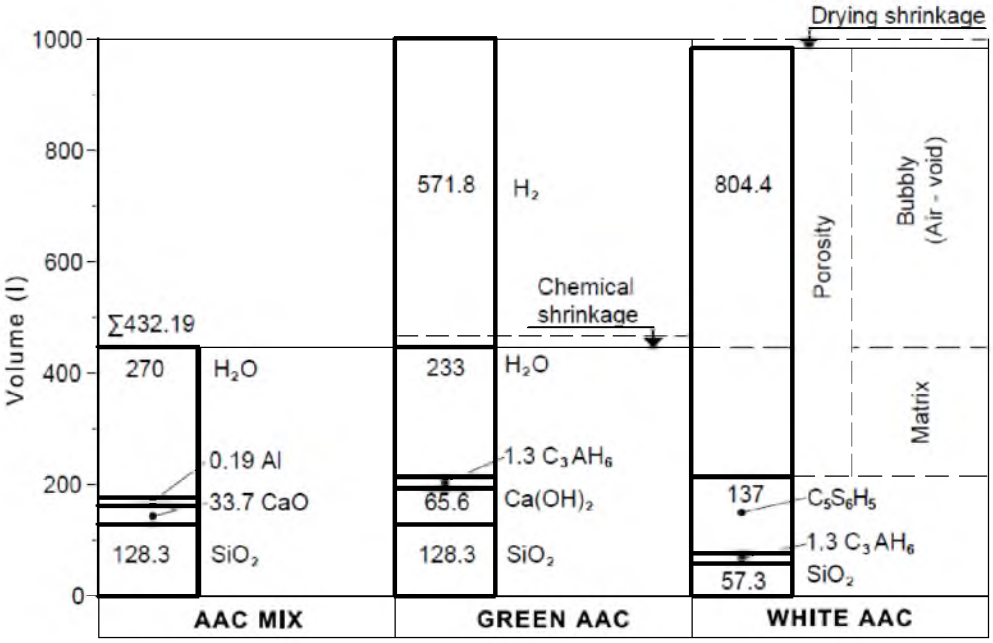

Figure 2. Phase composition and types of porosity per 1 m^3 of model freshly mix, green cake and white AAC D500: C_3AH_6 – abbreviated $3CaO{\cdot}Al_2O_3{\cdot}6H_2O$ according to cement as accepted in chemistry; the same, tobermorite $C_5S_6H_5$.

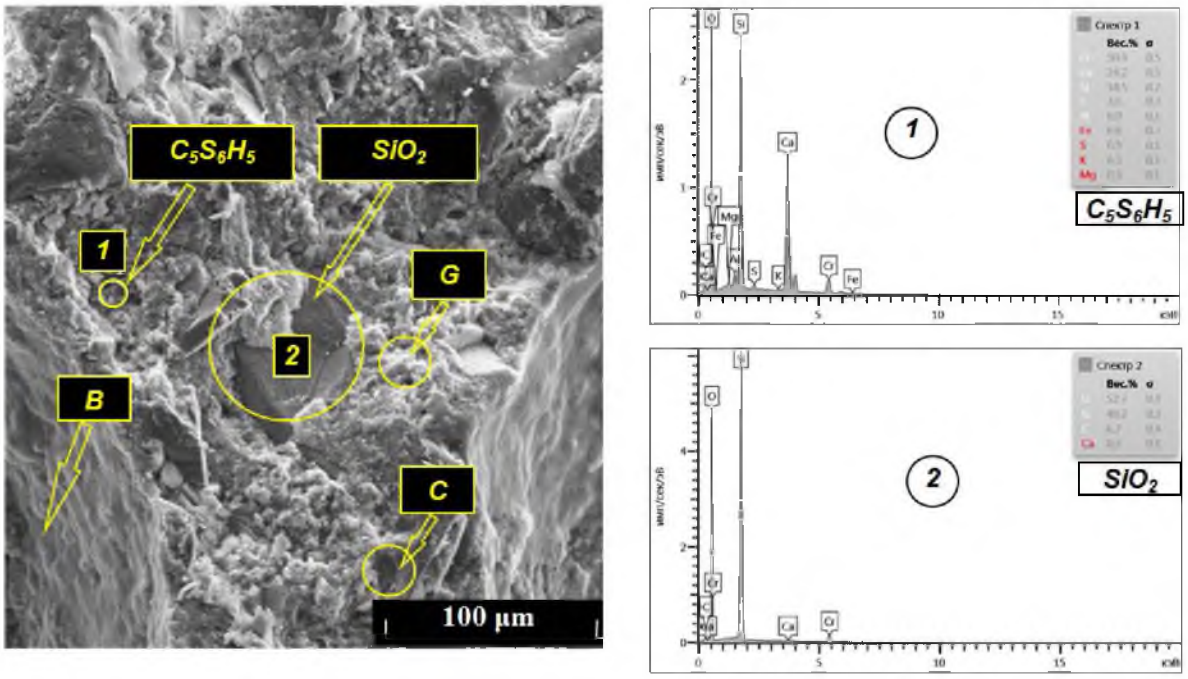

Figure 3. The structure of AAC D500: *G* – gel pores; *C* – capillary pores; *B* – bubbly air pores.

Area 1. Gel pores (Fig. 3, Fig. 4d). The gel porosity of calcium hydrosilicate was calculated according to the data of T. Powers [5] on its value in the gel of hardened systems, equal to 28 %. For the AAC D500 under consideration, a value of 53.3 liters was obtained. The specific volume of tobermorite growth is 0.569, which corresponds to the T. Powers model with a specific gel volume of 0.567. The size for gel pores was determined by IUPAC recommendation and proposal [20]: microgel with pore diameter (d_p) < 2 nm and mesogel with d_p from 2 to 50 nm.

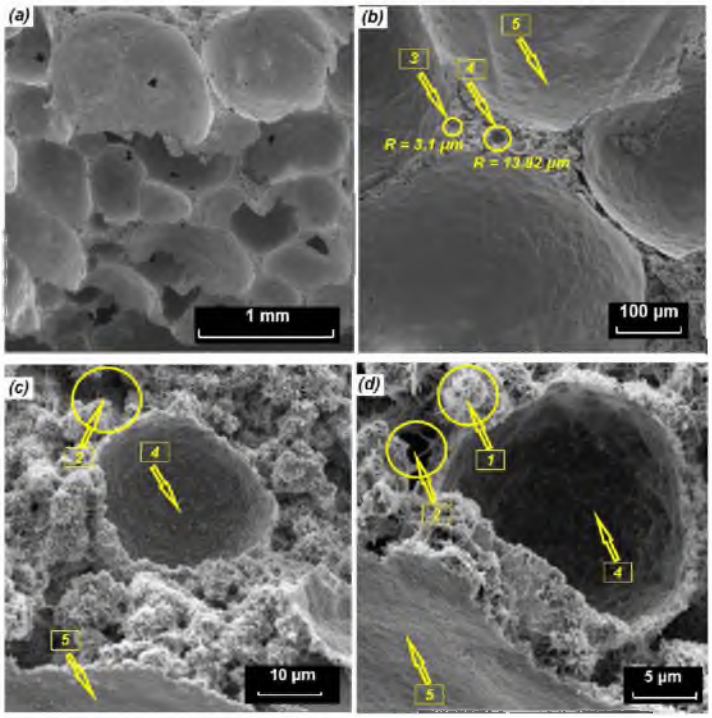

Figure 4. SEM micrographs of FC D250: *1* – gel pores; *2* – capillary pores; *3* – air-micro pores; *4* – air-membrane pores; *5* – air-cellular pores.

The second term in equation (3) for any type of cellular concrete and ingredients composition in the mix allows us to estimate the volume proportion of hydrated phases and to determine the expected value of gel porosity.

Area 2. Capillary pores (Fig. 3; Fig. 4 c, d). The capillary pores presence in concrete is caused by mixing water surplus compared to the quantity of chemically bonded water, as well as contraction phenomena during hardening. It is recommended that contraction porosity not be isolated but added to capillary pores. The equivalent diameter of microcapillary pores (in terminology [20]) is from 50 nm to 1 μm.

Gel pores and capillary pores are formed during hydration in a hardening system. Together with the solid phases of the system, these pores form a hardened matrix in concrete [45, 46]. Gel pores and capillary pores are matrix pores. The properties of AAC and FC, as well as ordinary concrete, depend on the nanostructure and the microstructure of cementitious materials [47, 48], that is, on the matrix structure.

Most pores in AAC and FC are pores of bubble origin. The pores in the structure of the hardened composite AAC, FC, and with entrained air are called air-void [49–53].

An examination of the characteristics of the bubbles in a fresh concrete mix with air-void sizes makes it possible to distinguish three types of bubbles: air-micro bubble, air-membrane bubble and air-cellular bubble. In the structure of AAC and FC, respectively, three areas of air pores formed from vesicles are distinguished.

Area 3. Air-capillary pores (Fig. 4b). The selection of this area is associated with transition in porous system structure from capillary pores to air-micro pores. The diameter of mesocapillary pores according to the terminology [20] and air-micro pores is from 1 to 10 μm. The pressure in the bubble with R * = 3.1 μm (Fig. 4b), caused by the surface curvature P_C = $2\sigma/R$, is R^*_C= $4.7 \cdot 10^4$ Pa. Bond number as gravity to surface tension ratio for the bubble under consideration Bo = $8.7 \cdot 10^{-6}$ << 1. Therefore, air-micro bubbles in a AAC and FC mixes are spherical and non-deformable.

Area 4. Air-membrane pores (Fig. 4b, c, d). Pores with a diameter from 10 to 100 μm are involved in partitions structure formation between larger air pores. In structural heat-insulating aerated concrete, the shape of bubble membrane pores is close to spherical, but can change to ellipsoidal.

In a hardened matrix, spherical air-micro pores are formed from spherical vesicles.

The binder particle size corresponds to the air-membrane pores size. The spherical air bubbles rise of the considered sizes in water, up to a constant, coincides with the Stokes formula for the solid sphere motion [54]. The geometric factor is the basis on which air bubbles from 10 to 100 μm in size, together with binder, filler and growth particles form the membrane structure in aerated concrete mix. Membrane bubbles

with a diameter less than 60 μm, as will be shown below, are classified as undeformable by the criterion of gravity to surface tension ratio.

Area 5. Air-cellular pores (Fig. 3 and 4) are basic in cellular concrete volume, predetermine the material name and its properties. The pore diameter is from 100 μm to 2 mm.

The air bubbles size upper limit in a cellular concrete mix D = 2 mm is determined from equality condition to the Bond number. The value Bo = 1 determines the region linear scale in which the surface tension and gravity are comparable and characterized by a capillary constant:

$$b = \sqrt{\frac{\sigma}{g\left(\rho_L - \rho_G\right)}}. \quad (4)$$

The capillary constant for the most liquids has a value of 1 ... 3 mm [46]. For a bubble in the model AAC mix under consideration, the capillary constant is b' = 2.11 mm. For water with σ = 7.27 · 10^{-2} J/m^2, the value of b'' = 2.72 mm. When deforming spherical bubbles, it is necessary to use the concept of "equivalent bubble", the volume of which is equal to the volume of the deformed one.

The following estimates are obtained for the lower boundary of the introduced size of air bubbles D = 0.1 mm. A air bubble of this size in a model AAC mix with a density of 1670 kg / m^3 as a unit cell has a Bond number Bo = 0.225 · 10^{-2} << 1. Capillary forces exceed the deforming gravitational (Archimedean) forces by more than two orders of magnitude, which corresponds to a gas bubble sphericity condition. Such an assessment is valid for a air bubble located at the AAC mix surface. Gravity forces from the overlying column of aerated concrete mix act on the bubble at the bottom of the form. If the hydrostatic pressures and laplace pressures are equal, the bubble radius according to equation (3) will be $R^* = 2 \cdot \sigma / \rho_{mix} \cdot g \cdot H$.

When a form in the manufacture of AAC with a height of 0.6 m is filled with the model aerated concrete mix under consideration, the filling height is H = 0.26 m and the deformable bubbles diameter will be more than 68.3 μm. An array height increase and a decrease in the surface tension in the mix due to surfactants will proportionally reduce the bubble size that is not deformed by calculation. Therefore, in AAC and FC mix, air bubbles with a diameter of 0.1 to 2 mm are stable, but deformable.

Large pores with an effective diameter of more than 2 mm are defects in the structure of AAC and FC. There are two reasons for their appearance in the hardened matrix. The first reason is the coalescence of bubbles in a fresh mix. The second reason is entrained air in a fresh mix. Air-entrained bubbles with d_p > 2 mm in AAC and FC take the shape of an inverted drop and retain this shape in the hardened composition.

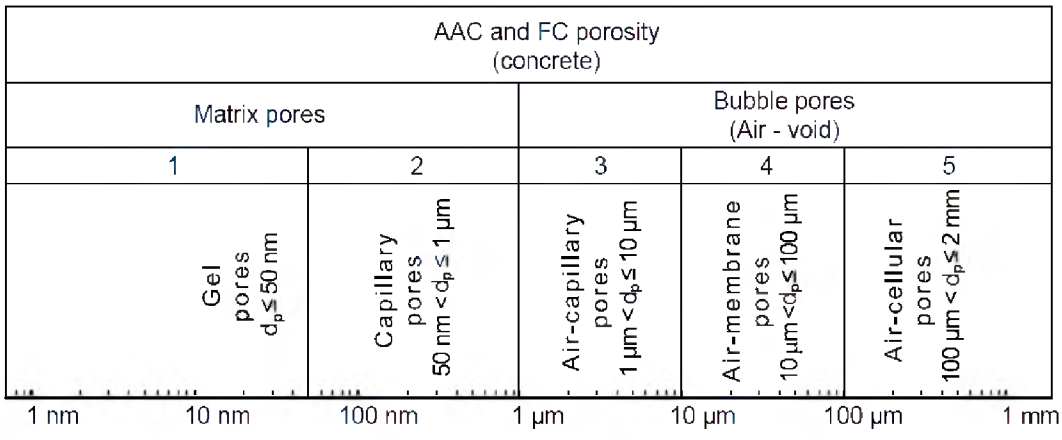

Figure 5. Kinds and sizes of pores in AAC and FC.

Fig. 5 provides information on the separation of vesicular pores into kinds. In this case, the mechanics data of a two-phase system were used for bubbles [37, 54]. An additional criterion for air pores separation by size was the same scale on the pore diameters axis with a logarithmic scale. The concept of gel and capillary pores in hardening systems is generally accepted [1, 7, 20, et. al.]. It is expedient to combine gel and capillary pores with the concept of "matrix pores", as is done in [4, 10]. There are only a few mentions of air-void pores as bubble pores in the literature [4]. The collection of bubble pores, named by origin, is divided into air-capillary, air-membrane and air-cellular pores. Subsequently, the isolated types of vesicular pores can be differentiated. So, air-membrane pores can be divided into formed by their undeformable and deformed bubbles in a fresh concrete mix.

Bubble studies are carried out mainly in cement foams with a bubble diameter of a millimeter size [55, 56]. In [56], the diameter of bubbles in monodispersed cement foams was 0.8 mm. This is close to the upper limit of the air-cellular pores size of 2 mm. In the systems of air-membrane pores with a bubble size from 10 μm to 100 μm, and especially for air-capillary pores with a diameter of 1 to 10 μm, new patterns are predicted. The new properties of such bubbles in solidifying systems with their predominant content in AAC and FC will be associated with the non-deformability of the bubble.

The data obtained and the proposed division by bubble pore sizes indicate the need for future studies of AAC and FC with a significant content, primarily, of non-deformable air-membrane pores.

4. Conclusions

The following conclusions can be made:

1. The main element of AAC and FC structure origin are bubble air pores. The technological process modeling in specific types of aeratedr concrete manufacture allows us to quantify the size of gel, capillary and bubble porosity in the material. The matrix porosity volume is determined by the mixing water amount remaining in the system after binder hydration, and is a smaller part of the total pore volume. In AAC D500 with W/S = 0.6, the matrix pore size is 29 %, and the bubble pore size is 71 %.

2. In porous hardening systems, three types of bubble pores are distinguished, the sizes of the selected pore areas are determined, and the shape of the bubbles is estimated. The air-capillary pores area with a size range from 1 to 10 μm is transitional from shapeless capillary to spherical microair pores. Membrane air pores with a diameter from 10 to 100 μm are comparable in size to the binder particles, and at a size of less than 60 μm, the bubbles in the fresh mix are classified as undeformable, and the pore form is close to spherical. Air-cellular pores with diameters from 100 μm to 2 mm are the main ones in the aerated concrete volume. They are formed from stable, but deformable in a AAC and FC mixture of air bubbles.

3. A perspective technology for aerated concrete is to reduce the maximum and average pore size for membrane and cellular air pores selected areas. A decrease in the bubbles size in hardening system will affect the decrease in the Bond number and increase the capillary forces importance in the AAC and FC pore structure formation.

5. Acknowledgements

This work was realized using the laboratory platform of the High Technology Center at BSTU named after V.G. Shukhov.

References

1. Krämer, C., Schauerte, M., Kowald, T.L., Trettin, R.H.F. Three-phase-foams for foam concrete application. Materials Characterization. 2015. 102. Pp. 173–179. DOI: 10.1016/j.matchar.2015.03.004
2. Smolczyk, H.G. Die Ettringit-Phasen im Hochofenzement. Zement-Kalk-Gips. 1961. 14. Pp. 277–284.
3. Lyu, K., She, W., Miao, C., Chang, H., Gu, Y. Quantitative characterization of pore morphology in hardened cement paste via SEM-BSE image analysis. Construction and Building Materials. 2019. 202. Pp. 589–602. DOI: 10.1016/j.conbuildmat.20-19.01.055
4. Zingg, L., Briffaut, M., Baroth, J., Malecot, Y. Influence of cement matrix porosity on the triaxial behaviour of concrete. Cement and concrete research. 2016. 80. Pp. 52–59. DOI: 10.1016/j.cemconres.2015.10.005
5. Powers, T.C., Brownyard, T.L. Studies of the physical properties of hardened Portland cement paste. Journal Proceedings. 1946. 43(9). Pp. 101–132.
6. Galan, I., Beltagui, H., Garc'ia-Maté, M., Glasser, F.P., Imbabi, M.S. Impact of drying on pore structures in ettringite-rich cements. Cement and Concrete Research. 2016. 84. Pp. 85–94. DOI: 10.1016/j.cemconres.2016.03.003
7. Hou, D., Li, D., Hua, P., Jiang, J., Zhang, G. Statistical modelling of compressive strength controlled by porosity and pore size distribution for cementitious materials. Cement and Concrete Composites. 2019. 96. Pp. 11–20. DOI: 10.1016/j.cemconcomp.2018.10.012
8. Zhou, S., Sheng, W., Wang, Z., Yao, W., Huang, H., Wei, Y., Li, R. Quick image analysis of concrete pore structure based on deep learning. Construction and Building Materials. 2019. 208. Pp. 144–157. DOI: 10.1016/j.conbuildmat.2019.03.006
9. Chung, S.-Y., Elrahman, M.A., Kim, J.-S., Han, T.-S., Stephan, D., Sikora, P. Comparison of lightweight aggregate and foamed concrete with the same density level using image-based characterizations. Construction and Building Materials. 2019. 211. Pp. 988–999. DOI: 10.1016/j.conbuildmat.2019.03.270
10. Bharadwaj, K., Glosser, D., Moradllo, M.K., Isgor, O.B., Weiss, W.J. Toward the prediction of pore volumes and freeze-thaw performance of concrete using thermodynamic modelling. Cement and Concrete Research. 2019. 124. Pp. 105820. DOI: 10.1016/j.cemconres.2019.105820
11. Chistyakov, B.Z., Mysatov, I.A., Bochkov, V.I. Proizvodstvo gazobetonnyh izdelij po rezatel'noj tekhnologii [Aerated concrete products production using cutting technology]. L.: Stroiizdat, 1977. p. 240. (rus)
12. Ramamurthy, K., Nambiar, E.K., Ranjani, G., Indu S. A classification of studies on properties of foam concrete. Cement and Concrete Composites. 2009. 31(6). Pp. 388–396. DOI: 10.1016/j.cemconcomp.2009.04.006

13. Kumar, E.M., Ramamurthy, K. Effect of fineness and dosage of aluminium powder on the properties of moist-cured aerated concrete. Construction and Building Materials. 2015. 95. Pp. 486–496. DOI: 10.1016/j.conbuildmat.2015.07.122
14. Narayan, N., Ramamurthy, K. Structure and properties of autoclaved aerated concrete: a review, microstructural investigations on aerated concrete. Cement and Concrete Research. 2000. 22. Pp. 321–329. DOI: 10.1016/S0958-9465(00)00016-0
15. Kurama, H., Topcu, I.B., Karakurt, C. Properties of the autoclaved aerated concrete produced from coal bottom ash. Journal of materials processing technology. 2009. 209(2). Pp. 767–773. DOI: 10.1016/j.jmatprotec.2008.02.044
16. Jerman, M., Keppert, M., V`yborn`y, J., Černˋy, R. Hygric, thermal and durability properties of autoclaved aerated concrete. Construction and building materials. 2013. 41. Pp. 352–359. DOI: 10.1016/j.conbuildmat.2012.12.036
17. Trong, L.N., Asamoto, S., Matsui, K. Sorption isotherm and length change behavior of autoclaved aerated concrete. Cement and Concrete Composites. 2018. 94. Pp. 136–144. DOI: 10.1016/j.cemconcomp.2018.09.003
18. Batool, F., Bindiganavile, V. Quantification of factors influencing the thermal conductivity of cement-based foam. Cement and Concrete Composites. 2018. 91. Pp. 76–86. DOI: 10.1016/j.cemconcomp.2018.04.015
19. Raj, A., Sathyan, D., Mini, K.M. Physical and functional characteristics of foam concrete: A review. Construction and Building Materials. 2019. 221. Pp. 787–799. DOI: 10.1016/j.conbuildmat.2019.06.052
20. Anders, N. Investigations about porosity analyzing of AAC. 6th International Conference on Autoclaved Aerated Concrete. 2018. 2(4). Pp. 141–145. DOI: 10.1002/cepa.895
21. Wei, S., Yiqiang, C., Yunsheng, Z., Jones, M.R. Characterization and simulation of microstructure and thermal properties of foamed concrete. Construction and building materials. 2013. 47. Pp. 1278–1291. DOI: 10.1016/j.conbuildmat.2013.06.027
22. She, W., Zhang, Y., Jones, M.R. Three-dimensional numerical modeling and simulation of the thermal properties of foamed concrete. Construction and Building Materials. 2014. 50. Pp. 421–431. DOI: 10.1016/j.conbuildmat.2013.09.027
23. Youssef, M. Ben, Lavergne, F., Sab, K., Miled, K., Neji, J. Upscaling the elastic stiffness of foam concrete as a three-phase composite material. Cement and Concrete Research. 2018. 110. Pp. 13–23. DOI: 10.1016/j.cemconres.2018.04.021
24. Pietras, D., Sadowski, T. A numerical model for description of mechanical behaviour of a Functionally Graded Autoclaved Aerated Concrete created on the basis of experimental results for homogenous Autoclaved Aerated Concretes with different porosities. Construction and Building Materials. 2019. 204. Pp. 839–848. DOI: 10.1016/j.conbuildmat.2019.01.189
25. Tarasov, A.S., Kearsley, E.P., Kolomatskiy, A.S., Mostert, H.F. Heat evolution due to cement hydration in foamed concrete. Magazine of concrete research. 2010. 62(12). Pp. 895–906. DOI: 10.1680/macr.2010.62.12.895
26. Adrien, J., Meille, S., Tadier, S., Maire, E., Sasaki, L. In-situ X-ray tomographic monitoring of gypsum plaster setting. Cement and Concrete Research. 2016. 82. Pp. 107–116. DOI: 10.1016/j.cemconres.2015.12.011
27. Jiang, J., Lu, Z., Li, J., Fan, Y., Niu, Y. Preparation and hardened properties of lightweight gypsum plaster based on pre-swelled bentonite. Construction and Building Materials. 2019. 215. Pp. 360–370. DOI: 10.1016/j.conbuildmat.2019.04.181
28. Wang, Q., Cui, Y., Xue, J. Study on the improvement of the waterproof and mechanical properties of hemihydrate phosphogypsum-based foam insulation materials. Construction and Building Materials. 2020. 230. Pp. 117014. DOI: 10.1016/j.conbuildmat.2019.117014
29. Vatin, N., Korniyenko, S.V, Gorshkov, A.S., Pestryakov, I.I., Olshevskiy, V. Actual thermophysical characteristics of autoclaved aerated concrete. Magazine of Civil Engineering. 2020. 96(4). Pp. 129–137. DOI: 10.18720/MCE.96.11
30. Korniyenko, S.V. Thermophysical field testing of residential buildings made of autoclaved aerated concrete blocks. Magazine of Civil Engineering. 2016. 4 (64). Pp. 10–25. DOI: 10.5862/MCE.64.2
31. Vatin, N.I., Gorshkov, A.S., Kornienko, S.V., Pestryakov, I.I. The consumer properties of wall products from AAC. Construction of Unique Buildings and Structures. 2016. (1). Pp. 78–101.
32. Gorshkov, A.S., Rymkevich, P.P., Vatin, N.I. Simulation of non-stationary heat transfer processes in autoclaved aerated concrete walls. Magazine of Civil Engineering. 2014. 52(8). Pp. 39–49. DOI: 10.5862/MCE.52.5
33. Jones, M.R., Ozlutas, K., Zheng, L. Stability and instability of foamed concrete. Magazine of Concrete Research. 2016. 68(11). Pp. 542–549. DOI: 10.1680/macr.15.00097
34. Krämer, C., Schauerte, M., Müller, T., Gebhard, S., Trettin, R. Application of reinforced three-phase-foams in UHPC foam concrete. Construction and Building Materials. 2017. 131. Pp. 746–757. DOI: 10.1016/j.conbuildmat.2016.11.027
35. Krämer, C., Kowald, T.L., Trettin, R.H.F. Pozzolanic hardened three-phase-foams. Cement and Concrete Composites. 2015. 62. Pp. 44–51. DOI: 10.1016/j.cemconcomp.2015.06.002
36. She, W., Du, Y., Miao, C., Liu, J., Zhao, G., Jiang, J., Zhang, Y. Application of organic-and nanoparticle-modified foams in foamed concrete: reinforcement and stabilization mechanisms. Cement and Concrete Research. 2018. 106. Pp. 12–22. DOI: 10.1016/j.cemconres.2018.01.020
37. Suleymanova, L.A., Pogorelova, I.A., Marushko, M.V. Theoretical Basis of Formation Highly Organized Porous Structure of Aerated Concrete. Materials Science Forum. 2019. 945. Pp. 309–317. DOI: 10.4028/www.scientific.net/MSF.945.309
38. Yu, Q.L., Brouwers, H.J.H. Microstructure and mechanical properties of $β$-hemihydrate produced gypsum: An insight from its hydration process. Construction and Building Materials. 2011. 25(7). Pp. 3149–3157. DOI: 10.1016/j.conbuildmat.20-10.12.005
39. Yu, Q.L., Brouwers, H.J.H. Development of a self-compacting gypsum-based lightweight composite. Cement and Concrete Composites. 2012. 34(9). Pp. 1033–1043. DOI: 10.1016/j.cemconcomp.2012.05.004
40. Li, P.P., Yu, Q.L., Brouwers, H.J.H., Chen, W. Conceptual design and performance evaluation of two-stage ultra-low binder ultra-high performance concrete. Cement and Concrete Research. 2019. 125. Pp. 105858. DOI: 10.1016/j.cemconres.20-19.105858
41. Koenig, A. Analysis of air voids in cementitious materials using micro X-ray computed (μXCT). Construction and Building Materials. 2020. 244. Pp. 118313. DOI: 10.1016/j.conbuildmat.2020.118313
42. Kim, J.-S., Chung, S.-Y., Han, T.-S., Stephan, D., Abd Elrahman, M. Modeling of multiple phase solid microstructures and prediction of mechanical behaviors of foamed concrete. Construction and Building Materials. 2020. 248. Pp. 118637. DOI: 10.1016/j.conbuildmat.2020.118637
43. Wong, H.S., Buenfeld, N.R. Determining the water-cement ratio, cement content, water content and degree of hydration of hardened cement paste: Method development and validation on paste samples. Cement and Concrete Research. 2009. 39(10). Pp. 957–965. DOI: 10.1016/j.cemconres.2009.06.013
44. Yio, M.H.N., Phelan, J.C., Wong, H.S., Buenfeld, N.R. Determining the slag fraction, water/binder ratio and degree of hydration in hardened cement pastes. Cement and concrete research. 2014. 56. Pp. 171–181. DOI: 10.1016/j.cemconres.20-09.06.013

45. Qu, X., Zhao, X. Previous and present investigations on the components, microstructure and main properties of autoclaved aerated concrete-A review. Construction and Building Materials. 2017. 135. Pp. 505–516. DOI: 10.1016/j.conbuildmat.2016.12.208
46. Liu, L., Qin, G., Qin, S., Tao, G. Simulation of the volumetric deformation and changes in the pore structure of unsaturated cement-based materials subjected to freezing/thawing. Construction and Building Materials. 2020. 230. Pp. 116964. DOI: 10.1016/j.conbuildmat.2019.116964
47. Snoeck, D., Pel, L., De Belie, N. Comparison of different techniques to study the nanostructure and the microstructure of cementitious materials with and without superabsorbent polymers. Construction and Building Materials. 2019. 223. Pp. 244–253. DOI: 10.1016/j.conbuildmat.2019.06.225
48. Wong, H.S., Poole, A.B., Wells, B., Eden, M., Barnes, R., Ferrari, J., Fox, R., Yio, M.H.N., Copuroglu, O., Gudhmundsson, G., others. Microscopy techniques for determining water-cement (w/c) ratio in hardened concrete: a round-robin assessment. Materials and Structures. 2020. 53(2). Pp. 1–19. DOI: 10.1617/s11527-020-1458-2
49. Kearsley, E., Visagie, M. Properties of foamed concrete as influenced by air-void parameters. Concrete Beton. 2002. 101. Pp. 8–14.
50. Nambiar, E.K.K., Ramamurthy, K. Air-void characterisation of foam concrete. Cement and concrete research. 2007. 37(2). Pp. 221–230. DOI: 10.1016/j.cemconres.2006.10.009
51. Aamr-Daya, E., Langlet, T., Benazzouk, A., Quéneudec, M. Feasibility study of lightweight cement composite containing flax by-product particles: Physico-mechanical properties. Cement and Concrete Composites. 2008. 30(10). Pp. 957–963. DOI: 10.1016/j.cemconcomp.2008.06.002/
52. Sypek, M., Latawiec Rafałand Pichór, W. Gypsum dehydration in cement and its impact on air-void structure in air-entrained concrete. Construction and Building Materials. 2019. 220. Pp. 396–402. DOI: 10.1016/j.conbuildmat.2019.06.011
53. 53. Wolter, S., Uhre, F.A.H., Hasholt, M.T., Dahl, V.A., Anton, F. Air void analysis of hardened concrete by means of photogrammetry. Construction and Building Materials. 2019. 226. Pp. 953–964. DOI: 10.1016/j.conbuildmat.2019.07.203
54. Labuntsov, D.A., Yagov, V.V. Mekhanika dvukhfaznykh system [Mechanics of two-phase systems]. M.: MEI, 2000. 374 p. (rus)
55. Petit, P., Javierre, I., Jézéquel, P.-H., Biance, A.-L. Generation and stability of bubbles in a cement based slurry. Cement and concrete research. 2014. 60. Pp. 37–44. DOI: 10.1016/j.cemconres.2014.02.008
56. Feneuil, B., Roussel, N., Pitois, O. Optimal cement paste yield stress for the production of stable cement foams. Cement and Concrete Research. 2019. 120. Pp. 142–151. DOI: 10.1016/j.cemconres.2019.03.002

Contacts:

Karina Kurochkina, karina200386@yandex.ru
Lyudmila Suleimanova, ludmilasuleimanova@ya.ru
Alexandr Kolomatsky, kolomatskiy@yandex.ru